Volume 1 | Number 1 | Jan 2013 | Pages 1–100

Journal of
Materials Chemistry A

Materials for energy and sustainability
www.rsc.org/materialsA

ROYAL SOCIETY
OF CHEMISTRY

ROYAL SOCIETY
OF CHEMISTRY

www.rsc.org/materialsA

Journal of Materials Chemistry A

COMMUNICATION

Graphitic Carbon Nitride Nano-Emitters on Silicon: a Photoelectrochemical Heterojunction Composed of Earth-Abundant Materials for Enhanced Evolution of Hydrogen
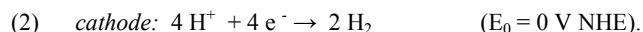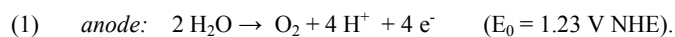
M. Lublow [a,b], A. Fischer [a], C. Merschjann [c], F. Yang [b], Th. Schedel-Niedrig [b], J.-F. Veyan [d], and Y. J. Chabal [d]

Graphitic carbon nitride is a promising heterogeneous catalyst for light-induced generation of hydrogen. Here, we report the successful formation of nano-scaled carbon nitride structures on silicon, mitigating the known limitations of charge transport within bulky C-N networks. An efficient photoelectrochemical heterojunction is thereby realized, developed from earth-abundant materials only.

The conversion of solar energy to chemical energy is one of the principal routes to establish a green global economy[1]. Particularly, hydrogen as a product of solar water splitting may assume a decisive role upon transition from fossil to renewable energy resources[2]. For realization of the solar-to-hydrogen conversion process by photoelectrochemical water splitting, suitable photoelectrodes still have to be developed and to meet important demands such as efficiency and durability. Most critical, electrode fabrication has to rely on cost-saving material consumption, and the use of earth-abundant materials appears inevitable for novel device architectures. In this respect, the combination of silicon and polymeric graphitic carbon nitride (g-C_3N_4) represents a highly attractive heterostructure, integrating a state-of-the-art photoabsorber and a promising photocatalyst. Silicon-based photoelectrodes on the one hand, already reached near-record efficiencies in light-induced evolution of hydrogen but had to be activated by noble-metal catalysts[3,4]. On the other hand, g-C_3N_4 is an established candidate for photocatalytic hydrogen production since the report of Wang et al. in 2008[5] which boosted almost instantaneously the interest in this material due to the prospect of solar fuel generation without use of noble metal catalysts[6-10].

[a]Technical University Berlin, Institute of Chemistry, Germany. [b]Helmholtz-Zentrum Berlin für Materialien und Energie, Institute Solar Fuels, Germany. [c]Universität of Rostock, Institute of Physics, Germany. [d]University of Texas at Dallas, Department of Materials Science and Engineering, USA.

Consistently, the substitution of noble-metal nanocontacts on silicon for the photocatalytic g-C_3N_4 appears to be a viable route to realize large-scale water splitting devices. This approach complements thereby current research trends where efficiency enhancement of carbon nitride is realized by heterojunctions with co-catalytic materials[11-13]. In powder form, the g-C_3N_4 photocatalyst necessitates the presence of sacrificial electron donors (triethanolamine for instance), in order to compensate for the charges consumed in the course of proton reduction. To overcome this limitation, the fabrication of macroscopic solid state (photo-) electrodes with compact g-C_3N_4 films was soon suggested[14,15]. In this latter approach, overall water splitting is realized under sustained operation in a photoelectrochemical cell, coupling an oxygen evolving anode via external circuitry to the carbon nitride cathode. Electrons consumed at the g-C_3N_4 electrode are thereby refilled by the counter reaction at the anode according to:

(1)   *anode:* $2\,H_2O \rightarrow O_2 + 4\,H^+ + 4\,e^-$ ($E_0 = 1.23$ V NHE).

(2)   *cathode:* $4\,H^+ + 4\,e^- \rightarrow 2\,H_2$ ($E_0 = 0$ V NHE).

Here, Eq. 1 describes the generation of four electrons upon oxygen evolution in acidic aqueous electrolytes at the anode which are thereby available at the g-C_3N_4 photocathode to reduce protons to hydrogen (Eq. 2). Standard potentials are indicated with respect to the Normal Hydrogen Electrode, NHE.

One important challenge with solid g-C_3N_4 films is to sufficiently maintain charge transport through the entire film structure: in 2010, Huda and Turner pointed to a bottleneck for electron (or hole) conduction within the heptazine-based C_3N_4-network[13], and, in fact, first solid state electrodes, equipped with micrometer-thick films, suffered from considerable attenuation of achievable maximum current densities[14,15]. Huda and Turner also concluded that light-induced electron-hole pairs may remain confined within the heptazine subunits[16] which could be later, to some extent, substantiated by analysis of time-resolved

photoluminescence spectra[17]. Modification of the g-C$_3$N$_4$ bulk geometry toward the nano-scale is therefore required to remedy these limitations.[18]

　　　In our approach, the obstacle of high film resistivity is resolved by down-scaling the g-C$_3$N$_4$ layer geometry to planar nano-sheets and -lamellae, respectively. Electron conduction toward the electrolyte (and hole conduction toward the support) is thereby realized almost without any detectable impediment. This improvement, however, does not seamlessly translate to the photoactivity of the nanoscaled films: the generation of usable light-induced charge carriers in the g-C$_3$N$_4$ layer alone still remains low, i.e. photocurrents of thin g-C$_3$N$_4$ films are only in the range of a few µAcm^{-2} while the photovoltage does not exceed some 10 mV. The employment of these nanostructures on top of (photoactive) silicon, however, turns out to be highly beneficial to fabricate an efficient heterojunction, otherwise only achievable by combination of silicon with noble-metal catalysts[3,4,19,20].

　　　In order to facilitate g-C$_3$N$_4$ film formation on silicon supports, boron and phosphor-doped substrates (doping density ~ 5 x 10^{15}cm^{-3}) with (100)-surface orientation were preconditioned by XeF$_2$ dry etching[21]. Surface analysis by scanning electron microscopy (SEM) and atomic force microscopy (AFM) is provided as Fig. 1 and proves the formation of a nano-structured surface, superimposed by ring-like craters on the micrometer-scale.
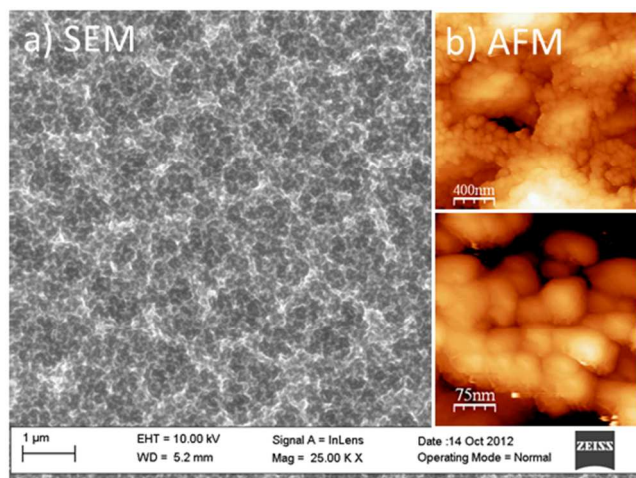

Fig. 1 XeF$_2$ dry etched silicon surface illustrated by SEM (a) and AFM (b). Two sequential etching steps by XeF$_2$ (gas pressure 3 Torr each) were applied to form the depicted surface morphology, constituted by cubic structures on the nano-scale and ring-shaped structures on the micrometer scale.

Subsequently, the surface was etched in concentrated hydrofluoric acid (50% HF) for several minutes to remove a remnant fluor-rich surface layer resulting from the dry etching process. Polymeric carbon nitride was deposited by polycondensation of dicyandiamide precursors under nitrogen atmosphere at 550° C[14,15]. The temperature in the preparation chamber was continuously increased at a rate of 20°C per minute and held constant for further 30 minutes at 550°C (preparation route 1). The thickness of the resulting surface films reached typically some 10 µm. The pronounced surface corrugation of the silicon support, obtained by XeF$_2$ dry

etching, helped minimizing inhomogeneities in the final g-C$_3$N$_4$ film structure, typically evolving upon transition of the intermediates melamine to melem between 210°C and 400°C. In order to further improve the adhesion to the substrate for selected samples, the intermediate liquid melamine film was mechanically smoothened by a spatula before the polycondensation process was continued. During this treatment, nitrogen was continuously directed into the preparation chamber but less protection of the samples against ambient air was achieved (preparation route 2). Finally, the entire g-C$_3$N$_4$/Si heterostructures were exposed to HF (50%) for incremented times of 10, 20 and 30 s, respectively. Topographical analysis by SEM proves the continued removal of the thick g-C$_3$N$_4$ layer from the silicon support by this treatment (see Fig. 2). After about 30 s, the surface coverage by g-C$_3$N$_4$ is only observable in the about one-micrometer sized ring-shaped craters of the Si substrate with layer thicknesses not exceeding a few 10 nm, i.e. the remaining carbon nitride material is fully embedded into the silicon surface topography (see supporting information and Figs. S1 – S3). The observed etching effect is assumed to occur by selective attack of the interfacial region between g-C$_3$N$_4$ and the silicon substrate, comprising Si and SiO$_2$, rather than by direct g-C$_3$N$_4$ etching. Such an interfacial oxide (SiO$_2$) is most probably forming upon contact of the aqueous solution of dicyandiamide with the support at elevated temperatures. At sites where the penetration of the etch solution toward the interface is impeded by an intimate, i.e., very dense carbon nitride – silicon contact, the etching effect proceeds much slower or is fully impeded, leaving behind the observed nano-sheets. Therefore, the HF-treatment can be conceived as chemical split-off of bulky g-C$_3$N$_4$-overlayers by underetching of the carbon nitride surface film.
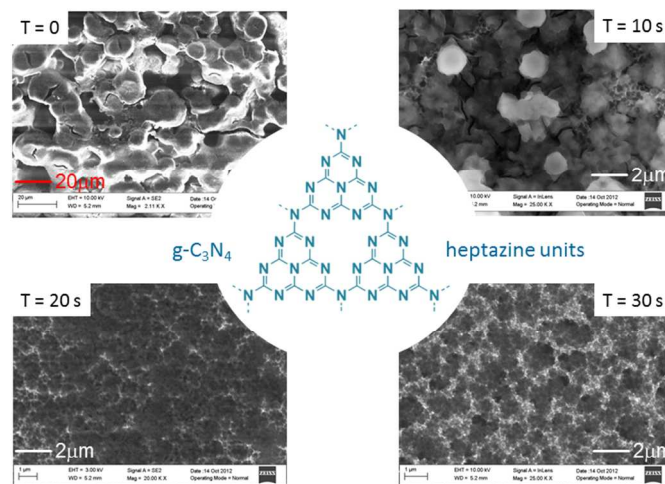

Fig. 2 Preparation of ultra-thin g-C$_3$N$_4$ structures on XeF$_2$ pre-etched silicon substrates. Etching in HF (50%) with incremented times leaves behind g-C$_3$N$_4$ nano-sheets embedded into the silicon surface topography while the bulky overlayer is removed. The center image depicts the idealized g-C$_3$N$_4$ molecular structure consisting of three heptazine subunits.

　　　The sample preparation according to route 2, including intermediate mechanical film smoothening, resulted in a different g-C$_3$N$_4$ morphology (see Fig. 3). After etching in HF (50%), the silicon substrate remained fully covered by carbon nitride, and the film structure is characterized by a multitude of

lamella-like nano-structures with varying orientation. SEM analysis is provided in Fig. 3 for two different length scales and detection angles. The large-scale image on the left, recorded by an electron detector inclined with respect to the surface normal, still reveals the underlying silicon topography (compare Figs. 1 and 3). The small-scale image on the right, recorded at identical electron acceleration energy (10 keV) but perpendicularly oriented with respect to the surface plane, shows the arrangement of nanometer-sized lamellae. It can be concluded that the connection to the substrate could be considerably enhanced by the intermediate smoothening step. The chemical composition of these nano-lamellae was assessed by X-ray photoelectron spectroscopy using a Mg-Kα X-ray source. In comparison to the corresponding XPS analysis of thick g-C$_3$N$_4$ films, an increased N-(C)$_3$ to C=N-C ratio is detected after deconvolution of the C 1s signal and suggests a closer resemblance to the stoichiometry of g-C$_3$N$_4$ powders[15].
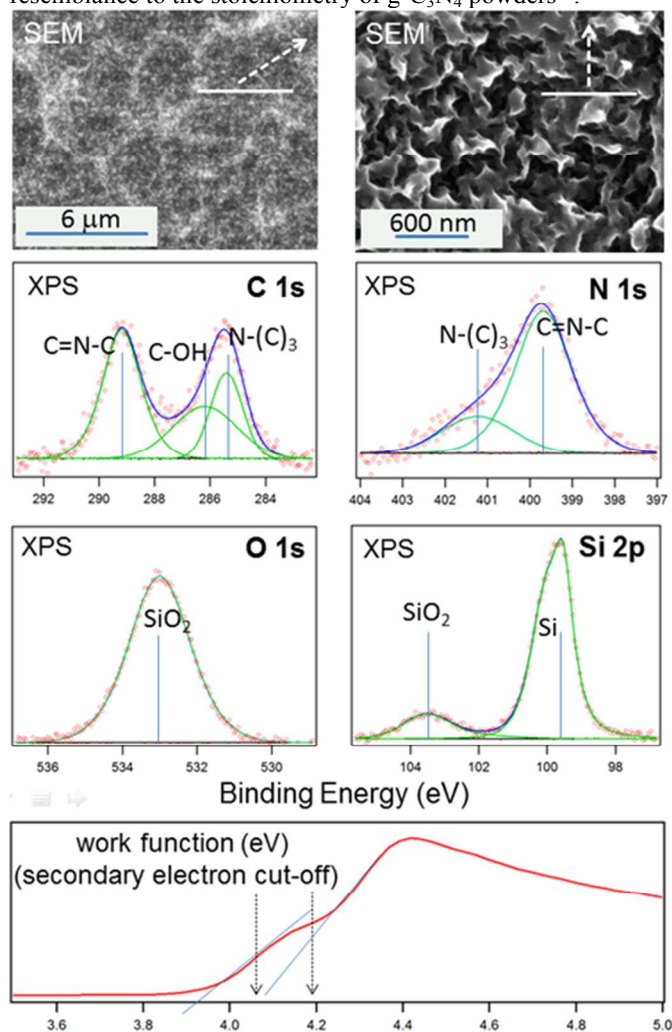

Fig. 3 SEM surface analysis and photoelectron spectroscopy results for g-C$_3$N$_4$ nano-lamellae on p-type silicon. Beside data for the C 1s, N 1s, O 1s and Si 2p core-level signals, also the cut-off region of secondary electrons is shown, measured at 1253.6 eV excitation energy and 5 V bias.

Additionally, a substructure near 286 eV can be attributed to the formation of C-OH. It appears likely that this compound is also present at the g-C$_3$N$_4$/Si interface and may account for the

improved adhesion to the support. Contributions of C=O carbonyl groups (at about 288 eV) to the overall signal are not distinguishable but cannot fully be excluded. Therefore, the intermediate contact of the sample to the ambient upon transition of melamine to melem appears not to modify the resulting stoichiometry in a pronounced way.

Deconvolution of the N 1s signal confirms the increased N-(C)$_3$ to C=N-C ratio while the Si 2p core-level signal proves the presence of oxidized silicon. Since the X-ray beam also probed areas of bare silicon at the boundary of the sample, the origin of the SiO$_2$ signal is not unambiguous and may result from both, the boundary region as well as from the interfacial region beneath the g-C$_3$N$_4$ film. The O 1s signal could be fitted by a single singlet function centered at 533 eV. This binding energy corresponds to both SiO$_2$ (in accordance to the deconvolution of the Si 2p curve) as well as to phenolic groups (in accordance to the C-OH signal in the C 1s curve)[22-24]. In comparison to published XPS data of g-C$_3$N$_4$, the results of Fig. 3 clearly suggest that the thin remaining film at the silicon surface has the compositional properties of graphitic polymeric carbon nitride. Similar results were obtained for samples, prepared by preparation route 1. The signal-to-noise ratio, however, was much lower due to the embedding of the nano-sheets into the silicon surface structure. The analysis of the XPS cut-off of secondary electrons, finally, shows an additional shoulder, pointing thereby to a variation of the surface potential across the detection area. Such a variation may be induced by regions with larger negative band bending or by a variation of the strength of an interfacial or surface dipole. The work function, i.e. the distance between the Fermi-level and the vacuum level, therefore cannot clearly be assigned and varies between about 4.2 eV and below 4.1 eV.
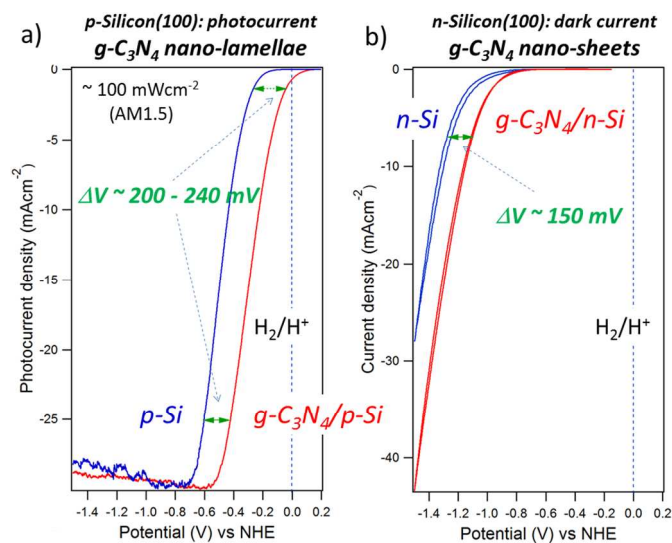
Fig. 4 Photocurrent (with p-type Si substrate) and dark current behavior (with n-type Si substrate) of g-C$_3$N$_4$/Si heterojunctions were measured in 1M H$_2$SO$_4$. Improvements in the photocurrent behavior by the g-C$_3$N$_4$ nano-structured films are indicated by corresponding potential shifts, ΔV.

In order to evaluate the photoelectrochemical efficiency of the g-C$_3$N$_4$ layer alone, thin g-C$_3$N$_4$ films were prepared on non-photoactive substrates of fluorinated tin oxide (FTO) and tested for light-induced evolution of hydrogen. As electrolyte

1M H_2SO_4 (pH0) was used. Since the above described method of chemical split-off is not applicable to the combination of g-C_3N_4 with FTO, mechanical thinning by continued polishing with abrasive material had to be carried out. The photovoltage of these films, determined by the difference of the open circuit potential in the dark and under illumination, was in the range between 20 and 60 mV. Photocurrents, determined as the corresponding difference of current densities in the dark and under illumination at the standard potential for hydrogen evolution ($E_0 = 0$ V) reached only about 1 μAcm^{-2}. Direct evidence for the evolution of hydrogen under AM1.5 conditions was proven by differential electrochemical mass spectroscopy (DEMS). Further details are provided as supporting information (see Figs. S6 – S8). Since both anodic and cathodic photocurrents were observed for different samples, we conclude that the g-C_3N_4 – electrolyte interface (at pH0) is characterized by near flat-band conditions, i.e. small (chemical) changes at the g-C_3N_4 surface reverse a small downward band bending (accelerating light-induced electrons toward the surface) to an upward band bending (accelerating light-induced holes toward the surface).

The photoelectrochemical performance of the g-C_3N_4/Si heterojunction was assessed after preparation of nano-sheets (preparation route 1) and nano-lamellae (preparation route 2) on

p-type Si(100). Results for g-C_3N_4 nano-lamellae on p-type Si are shown in Fig. 4a. The blue curve characterizes the photoelectrode behaviour of the XeF_2 dry etched surface before deposition of g-C_3N_4. The current onset of -0.24 V NHE (determined by the potential corresponding to about 1 $mAcm^{-2}$) is shifted in negative direction with respect to the standard potential E_0. Saturation photocurrent densities of about 30 $mAcm^{-2}$ are reached near -0.78 V NHE, corresponding to the maximum photon-to-charge-carrier conversion under AM1.5 illumination conditions (100 $mWcm^2$). After preparation of g-C_3N_4 nano-lamellae, the current onset is shifted toward more positive values (to 0.0 V NHE), i.e. hydrogen is evolving already with a current density of 1 $mAcm^{-2}$ directly at E_0. The magnitude of the saturation photocurrent density remains the same suggesting thereby that incident light can pass the carbon nitride layer without considerable attenuation. The onset of the saturation photocurrent is located at -0.58 V NHE and therefore shifted by about 200 mV with respect to the bare support. On average, both curves are mutually shifted by 200 – 240 mV. With g-C_3N_4 nano-sheets, the above results could be confirmed. The overall improvement, however, fell below 200 mV, i.e. the mutual shift between the curves of the bare substrate and the nano-sheet covered substrate ranged between 140 and 180 mV.
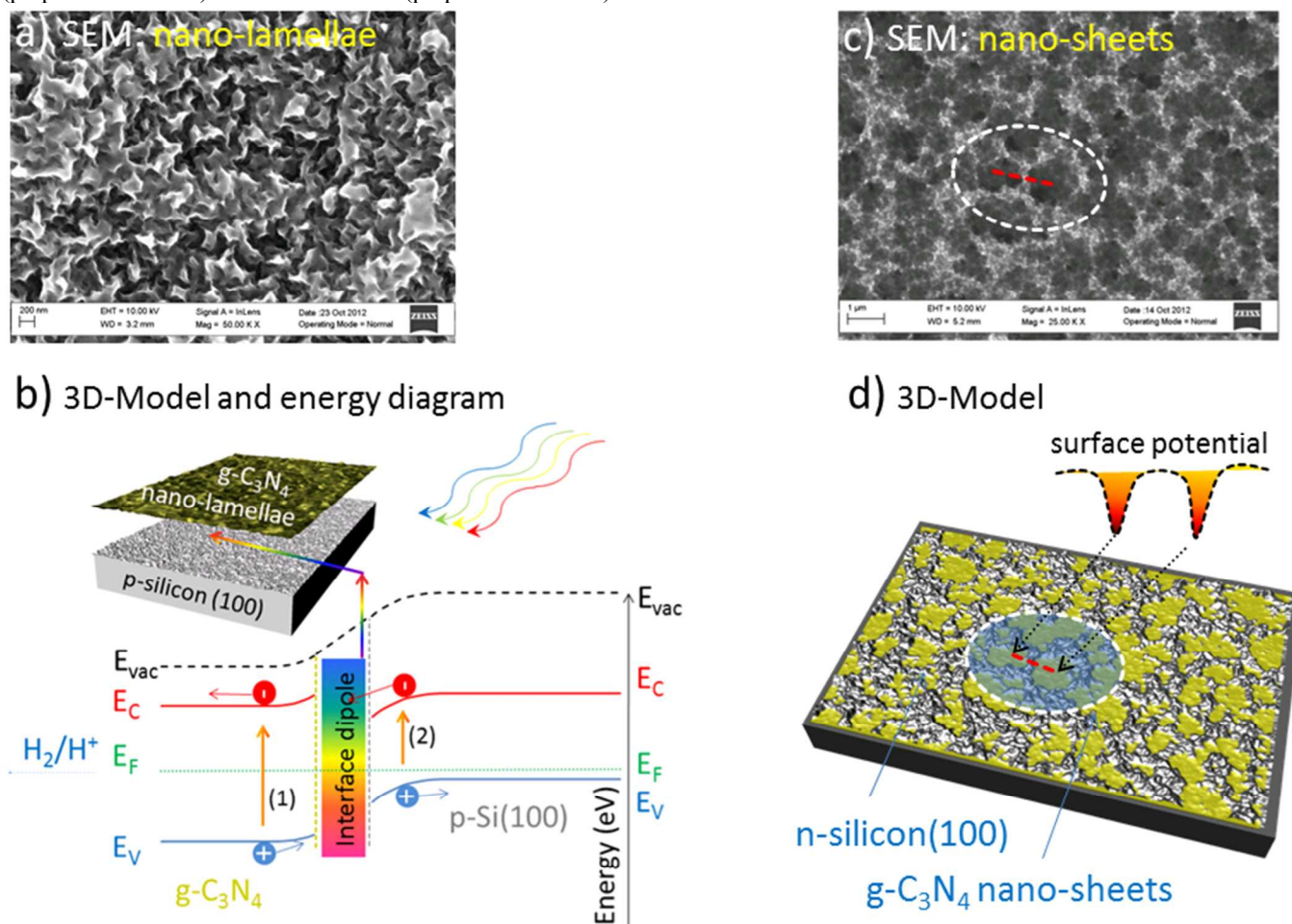

Fig. 5 SEM surface images of g-C_3N_4 nano-lamellae (a) and nano-sheets (c) and corresponding energy diagrams of the g-C_3N_4/p-Si interface region (b) and the g-C_3N_4/n-Si surface region (d). The energy diagram in (b) describes the variation of the potential energy for electrons perpendicular to the heterojunction. The presence of an interfacial dipole layer is indicated by corresponding arrows. In (c) and (d), the variation of the surface potential parallel to the surface refers to the indicated red dashed line.

Corresponding results after preparation of nano-sheets on p-Si(100) are provided as supporting information (see Fig. S5). Mass spectroscopic detection of hydrogen confirms that, in fact, the observed photocurrents have to be attributed to the reduction of protons at the surface of the photoelectrodes (see Fig. S8).

Finally, in order to analyze the junction properties independently from light-induced charge carrier generation, the current-voltage characteristic was also determined after formation of g-C_3N_4 nano-sheets and nano-lamellae on n-type Si(100) substrates. Similar results were obtained for both g-C_3N_4 morphologies and Fig. 4b summarizes only the results for the nano-sheet structures. Here, the mutual shift of the curves amounts to about 150 mV. Overpotentials in the range of 1 V, however, remain extremely high but are typical for n-type Si. Since these measurements were carried out in the dark, the observed improvement emphasizes the importance of the electronic properties at the g-C_3N_4/Si interface to be discussed below. Stability for evolution of hydrogen was finally tested for all p-Si based heterojunctions at constant potentials where saturation photocurrents were reached (V < -0.8 V). During three hours of operation no change in performance was observed.

The observed findings confirm that the g-C_3N_4/Si heterojunction combines, as a whole, catalytic and semiconductor properties in a promising way. The efficiency of the bare silicon substrate for hydrogen is notably low. From a theoretical point of view, any enhancement of this efficiency depends, firstly, on the equilibration of the band structure at the g-C_3N_4/Si interface and, secondly on the (photo-)catalytic properties of the top-surface g-C_3N_4 layer. For the latter, the individual analysis of g-C_3N_4 thin films on FTO suggested detectable but low photoelectrocatalytic activity for the evolution of hydrogen (it should be noted that this result is most likely very specific to the applied preparation route via polycondensation). Therefore, the band alignment between both materials appears to be the most decisive factor that can account for the observed enhancement. In fact, the theoretical Fermi-level positions of silicon (about 4.3 eV for n-type and 4.9 eV for p-type silicon with respect to the vacuum level and for doping densities of about $10^{15} cm^{-3}$) let expect a large negative band bending within the silicon support and therefore a considerable driving force for light-generated electrons toward the g-C_3N_4 layer. There is, however, a large difference of the respective conduction band edges of about 1.4 eV (E_C of Si is located at 4.05 eV, while E_C of g-C_3N_4 is located between 2.6 and 3.0 eV[8,14,15,17]). Such a band discontinuity represents an additional energy barrier which can necessitate a corresponding high overpotential unless there is an interfacial dipole that lowers this barrier. In fact, the band alignment between silicon and the g-C_3N_4 nanostructures appears to occur without pronounced discontinuity at the conduction band edges. This conclusion is deduced from the improved onset of the photocurrent of the heterostructure in comparison to the substrate (Fig. 4). Consequently, the built-in potential, induced by equilibration of the respective Fermi-levels, is mostly determined by the difference of the work functions of p-type silicon (and n-type silicon, respectively) and of the polymeric carbon nitride ($E_F \sim 4.0$ eV). The observed improvement for p-type silicon in the range between 200 and 240 mV, however, remains below the theoretical difference of the respective Fermi-levels and may point to a more complex electronic situation at the g-C_3N_4/Si interface. Residual defect states at the silicon surface, for instance, or those forming upon carbon nitride deposition[25] are presumably impeding the theoretical maximum band bending and thereby the highest possible built-in potential. Despite this imperfection, the polymeric carbon nitride structures assume a role typically realized by noble-metal nanoparticles, i.e. g-C_3N_4 allows forming a rectifying heterojunction which accelerates electrons, light-generated in the silicon support, toward the g-C_3N_4/Si interface. Moreover, the non-metallic g-C_3N_4 nanostructures appear to be sufficiently conductive in order to promote transfer of the charges to the electrolyte. Although electron transport is probably strongly suppressed along the polymer chains[16] (i.e., within the graphitic sheets), finite conductivity perpendicular to the polymer sheets may occur due to the overlap of aromatic pi-orbitals (some indications are given in Ref. 17).

The proposed mechanism of band alignment between g-C_3N_4 and silicon is finally depicted in Fig. 5. The case of g-C_3N_4 nano-lamellae on p-type silicon, fully covering the silicon surface, is shown as (a) and (b), assuming the presence of an interfacial dipole that lowers the discontinuity of the respective conduction band edges of Si and g-C_3N_4. There are two routes of electron-hole pair generation by light absorption, indicated by corresponding arrows (1) and (2). Light absorption within the g-C_3N_4 layer (1) is, according to the preceding results, presumably negligible. Therefore, charge-carrier generation by light absorption within the silicon substrate (2) will mainly contribute to the overall photocurrent density. The induced band bending is such that electrons will be accelerated toward the g-C_3N_4 – electrolyte interface. Flat band conditions of the g-C_3N_4 layer were assumed, i.e. there is almost no band bending at the g-C_3N_4 – electrolyte interface. The case of only partial g-C_3N_4 coverage by g-C_3N_4 nano-sheets on n-type silicon introduces additional potential modulation across the surface. The conditions at the g-C_3N_4/Si interface are similar to those depicted in (b) but are characterized by a lower band bending due to the higher Fermi-level position in the n-doped substrate. In (c) and (d) it is assumed that the shown energy diagram also holds for the potential variation across the surface, i.e. there is an additional driving force for electrons parallel to the surface, pointing from regions of bare silicon to g-C_3N_4-covered areas.

Conclusions

Under-etching of polymeric carbon nitride bulk films appears to be a viable route for preparation of ultra-thin g-C_3N_4 coverage on photo-responsive substrates. By this chemical split-off technique only the most adhesive structures are left on the surface which is a prerequisite for efficient charge transfer across the heterojunction toward the electrolyte. We investigated the electrochemical behaviour for nanostructures, not fully covering the surface as well as lamellae-like closed films. Almost no influence of the resistive surface layer on the overall current density was observed, pointing to a fast charge transfer mechanism across the junction. As alternative for noble-metal nanocontacts, widely used for photocathodes of Schottky-type, however, the induced band bending in the substrate has to be further improved. We will address this challenge by variations of the g-C_3N_4 preparation route as well as by engineering of the g-C_3N_4/Si interface.

Journal of Materials Chemistry A Accepted Manuscript

References

1   C.-J. Winter, J. Nitsch (Eds.), „Hydrogen as an Energy Carrier – Technologies, Systems, Economy", Springer-Verlag Berlin Heidelberg 1988.

2   M. Ball, M. Wietschel (Eds.), „The Hydrogen Economy – Opportunities and Challenges", Cambridge University Press 2009.

3   S. W. Boettcher, E. L. Warren, M. C. Putnam, E. A. Santori, D. Turner-Evans, M. D. Kelzenberg, M. G. Walter, J. R. McKone, B. S. Brunschwig, H. A. Atwater, N. S. Lewis, J. Am. Chem. Soc. 2011, **133**, 1216.

4   S. W. Boettcher, J. M. Spurgeon, M. C. Putnam, E. L. Warren, D. Turner-Evans, M. D. Kelzenberg, M. G. Walter, J. R. Maiolo, H. A. Atwater, N. S. Lewis, Science 2010, **327**, 185.

5   X. Wang, K. Maeda, A. Thomas, K. Tokanabe, G. Xin, J. M. Carlsson, K. Domen, M. Antonietti, Nat. Mater. 2009, **8**, 76.

6   Y. Zheng, J. Liu, J. Liang, M. Jaroniec, S.Z. Qiao, Energy Environ. Sci. 2012, **5**, 6717.

7   S. C. Yan, S. B. Lv, Z. S. Li, Z. G. Zou, Dalton Trans. 2010, **39**, 1488.

8   X. Wang, X. Chen, A. Thomas, X. Fu, M. Antonietti, Adv. Mater. 2009, **21**, 1609.

9   Schwinghammer, K.; Tuffy, B.; Mesch, M. B.; Wirnhier, E.; Martineau, C.; Taulelle, F.; Schnick, W.; Senker, J.; Lotsch, B. V. Angew. Chem., Int. Ed. 2013, **52**, 2435.

10   K. Maeda, X. Wang, Y. Nishihara, D. Lu, M. Antonietti, K. Domen, J. Phys. Chem. C 2009, **113**, 4940.

11   Y. Hou, Y. Zhu,Y. Xu, X. Wang, Appl. Catal.B 2014, **156-157**, 122.

12   S. Zhou,Y. Liu, J. Li, Y. Wang, G. Jiang, Z. Zhao, D. Wang, A. Duan, J. Liu, Y. Wie, Appl. Catal. B 2014, **158-159**, 20.

13   V. Di Notoa, E. Negroa, S. Polizzib, K. Vezzùd, L. Toniolob, G. Cavinatoa, Int. J. Hydrogen Energy 2014, **39**, 2812.

14   F. Yang, M. Lublow, S. Orthmann, C. Merschjann, T. Tyborski, M. Rusu, S. Kubala, A. Thomas, R.Arrigo, M. Hävecker, T. Schedel-Niedrig, ChemSusChem 2012, **5**, 1227.

15   F. Yang, V. Kuznietzov, M. Lublow, C. Merschjann, A. Steigert, J. Klaer, T. Schedel-Niedrig, J. Mat. Chem. A 2013, **1**, 6407.

16   M. N. Huda, J. A. Turner, J. Appl. Phys. 2010, **107**, 123703.

17   C. Merschjann, T. Tyborski, S. Orthmann, F. Yang, K. Schwarzburg, M. Lublow, M.-C. Lux-Steiner, T. Schedel-Niedrig, Phys. Rev B 2013, **87**, 205204.

18   D. Hollmann, M. Karnahl, S. Tschierlei, K. Kailasam, M. Schneider, J. Radnik, K. Grabow, U. Bentrup, H. Junge, M. Beller, S. Lochbrunner, A. Thomas, A. Brückner, Chem. Mater. 2014, **26**, 1727.

19   Y. Nakato, H. Yano, S. Nishiura, T. Ueda, H. Tsubomura, J. Electroanal. Chem. 1987, **228**, 97.

20   Y. Nakato, H. Tsubomura, Electrochim. Acta 1992, 37, 897.

21   J.-F. Veyan, D. Aureau, Y. Gogte, P. Campbell, X.-M. Yan, and Y. J. Chabal, J. Appl. Phys. 2010, **108**, 114913.

22   F.J. Himpsel, F.R. McFeely, A. Taleb-Ibrahimi, J.A. Yarmoff, Phys. Rev. B, 1988, **38**, 6048.

23   H. C. Schniepp, L. J. Li, M. J. McAllister, H. Sai, M. Herrera-Alonso, D. H. Adamson, R. K. Prudhomme, R. Car, A. D. Saville,, A. I. Aksay, J. Phys. Chem. B 2006, **110**, 8535.

24   C. Hontoria-Lucas, A. J. Lopez-Peinado, J. D. López-Gónzalez, M. L. Rojas-Cervantes, R. M. Martin-Aranda, Carbon 1995, **33**, 1585.

25   M. Shaloma,, S. Inal, D. Neherb, M. Antonietti, Catalysis Today 2014, **225**, 185.

Journal of Materials Chemistry A Accepted Manuscript